$Au^{197}(n,\gamma)Au^{198}$ Reaction Mechanism*

O. A. WASSON, R. E. CHRIEN, M. R. BHAT, M. A. LONE,† AND M. BEER‡
Brookhaven National Laboratory, Upton, New York
(Received 21 March 1968)

The variation in intensity of 24 γ rays emitted in neutron capture near the 4.9-eV resonance in gold was measured as a function of neutron energy. Significant interference was observed in the partial capture cross sections, which was consistent with interference between local resonances provided that a bound level was postulated which contributes 3.5 b to the thermal-capture cross section. With this assumption, no direct-reaction mechanism is required in the capture process. Capture γ-ray spectra were also observed in the various resonances for neutron energies <400 eV. Previously unreported γ rays were observed in thermal-neutron capture, while additional new γ rays were observed in resonance capture. The choice of relative signs of the partial-width amplitudes of the 4.9- and 60-eV resonances required to fit the data is inconsistent with the usual assumption of normally distributed width amplitudes.

I. INTRODUCTION

THE observation of narrow resonances in the cross section for radiative capture of low-energy neutrons in gold is evidence that the reaction proceeds via a compound-nuclear process in which a long-lived ($\sim 10^{-15}$ sec) complex unbound state is formed. On the other hand, the intensities of the high-energy γ rays ($E_\gamma > 4.5$ MeV) emitted from thermal-neutron capture are larger than that expected from the statistical model[1] which assumes that the average γ-ray spectrum is independent of the specific nuclear-structure properties of the final states. The existence of this "anomalous" γ-ray spectrum requires a further investigation of the neutron-capture reaction mechanism in gold. For gold this anomalous spectrum was observed to exist from thermal- to 4-MeV neutron energies.[2] The failure to observe the anomalous γ-ray spectrum in the inelastic scattering of neutrons[3] from gold for excitations near the binding energy was given as evidence that some noncompound-nucleus interaction was responsible for the capture process since the inelastic scattering was a compound-nuclear process. The anomalous γ-ray spectrum was also observed in a reaction of the direct type. The $(d,p\gamma)$ experiments of Bartholomew *et al.*[4] showed an intense bump in the γ-ray spectrum at ~ 5 MeV for neutrons populating states near the neutron binding energy. The absence of a marked correlation between the size of the γ-ray gross structure bump with the location of the single-particle s and d states was given as evidence that the reaction was not a simple direct type, but perhaps involved a more complex doorway state[5] process. Starfelt[2] was unable to reproduce the γ-ray spectrum produced by kilovolt capture using any reasonable level-density formula with a partial radiation width proportional to E_γ^3. However, he obtained reasonable agreement with the data by extrapolating the $E1$ giant resonance to lower energies using the formula given by Axel[6] and by also including an $M1$ resonance at 5.5 MeV. Anomalously strong high-energy γ rays from thermal capture have also been observed in many elements in the mass regions $A<70$ and $180<A<208$, where the $2p$ and $3p$ single-particle states lie near the ground state.[7] This observation led to the consideration of the neutron-capture reaction as a simple direct type[8–10] in which the initial state consisted of an S-wave neutron coupled to the target nucleus. The neutron then undergoes a single-particle transition to a low-lying p state in the product nucleus by emitting dipole radiation. However, for gold the calculated direct-capture cross sections[8] were too small to explain the observed thermal γ-ray spectrum.

In spite of the unfavorable predictions of theory, several attempts were made to measure the direct-capture cross section in gold.[11–14] The procedure was to look for interference between direct and resonance radiative neutron capture near the 4.9-eV resonance in gold. The upper limits on the direct-capture cross sec-

* Work supported by the U. S. Atomic Energy Commission.
† Present address: Physics Department, University of Indiana, Bloomington, Ind.
‡ Guest Research Associate from State University of New York at Stony Brook, Stony Brook, N. Y.
[1] I. Bergqvist and N. Starfelt, Nucl. Phys. **39**, 353 (1962).
[2] N. Starfelt, Nucl. Phys. **53**, 397 (1964); B. Lundberg and N. Starfelt, *ibid.* **67**, 321 (1965).
[3] I. Bergqvist, B. Lundberg, L. Nilsson, and N. Starfelt, Nucl. Phys. **80**, 198 (1966); J. L. Perkin and N. Starfelt, *ibid.* **63**, 526 (1965).
[4] G. A. Bartholomew, E. D. Earle, A. J. Ferguson, and I. Bergqvist, Phys. Letters **24B**, 47 (1967).
[5] B. Block and H. Feshbach, Ann. Phys. (N. Y.) **23**, 47 (1963).
[6] P. Axel, Phys. Rev. **126**, 671 (1962).
[7] L. V. Groshev, A. M. Demidov, V. N. Lutsenko, and V. I. Pelekhov, in *Proceedings of the Second United Nations International Conference on the Peaceful Uses of Atomic Energy, Geneva, 1958* (United Nations, Geneva, 1958), Vol. 15, p. 138.
[8] A. M. Lane and J. E. Lynn, Nucl. Phys. **17**, 586 (1960).
[9] C. K. Bockelman, Nucl. Phys. **13**, 205 (1959).
[10] H. Morinaga and C. Ishii, Progr. Theoret. Phys. (Kyoto) **23**, 161 (1960).
[11] O. A. Wasson and J. E. Draper, Phys. Letters **6**, 350 (1963).
[12] D. Dorchoman, B. Kardon, D. Kish, and G. Samosvat, Zh. Eksperim. i Teor. Fiz. **46**, 1578 (1964) [English transl.: Soviet Phys.—JETP **19**, 1067 (1964)].
[13] V. D. Huynh, S. de Barros, J. Julien, G. Le Poittevin, J. Morgenstern, and C. Samour, in *Proceedings of the International Conference on the Study of Nuclear Structure with Neutrons, Antwerp, 1965* (North-Holland Publishing Co., Amsterdam, 1966).
[14] K. J. Wetzel, C. K. Bockelman, and O. A. Wasson, Nucl. Phys. **92**, 696 (1967).

tion reported by these experiments were too small to explain the anomalous γ-ray spectrum. However, these experiments used NaI γ-ray detectors which were unable to resolve individual γ rays and thus could only observe the behavior of a group of transitions. Although the interference effects of individual γ rays could be large, the observed interference for a group of transitions could be small because of mutual cancellation.

The purpose of the present experiment was to continue the search for direct neutron capture in gold by using Ge(Li) γ-ray detectors in order to resolve individual γ-ray transitions. The procedure was to again search for interference effects with the 4.9-eV resonance by measuring the variation in intensity of individual γ rays in the energy interval 1–40 eV. In addition, the γ-ray spectra from several resonances were obtained, and new energy levels in Au^{198} were deduced.

II. EXPERIMENTAL ARRANGEMENT

The experiment was performed at the fast-chopper facility[15] at the Brookhaven high flux beam reactor. The chopper speed was 6000 rpm which produced a 12 μsec full width at half-maximum (FWHM) burst of neutrons with a repetition rate of 400 pulses/sec. This chopper speed was selected as the best compromise between the desire for higher speed for improved neutron energy resolution at 100 eV and the desire for low speed with a large chopper transmission function at 0.6 eV. The neutron energies incident on the gold sample were determined by the time-of-flight technique using the 22-m flight path with a resultant neutron energy resolution of 0.5 μsec/m. The $3\times3\times\frac{1}{8}$-in. gold sample was oriented at 45° to the neutron beam to yield a thickness of 0.027 atoms/b. The γ-ray detector consisted of a 4-cc planar Ge(Li) diode. In order to reduce the background produced by neutrons scattered from the sample, a $\frac{1}{8}$-in. sheet of lead and $\frac{1}{4}$ in. of Li^6 were placed between the sample and detector holder. As has been described in a previous publication,[16] the pulse amplitude and flight time of each event were recorded on magnetic tape and subsequently analyzed at the central computer facility. In order to eliminate flight-time-dependent gain shifts, double *RC* differentiation was used in the main amplifier. A total of 3 days running time was devoted to the main gold experiment, while an additional day was spent on background measurements and γ-ray energy calibrations. Only those events which deposited energies greater than 2.0 MeV in the Ge(Li) detector were recorded. The γ-ray energy resolution for the summed spectra at 6.5 MeV was 7.6 keV, FWHM.

[15] R. E. Chrien and M. Reich, Nucl. Instr. Methods **53**, 93 (1967).

[16] M. R. Bhat, B. R. Borrill, R. E. Chrien, S. Randowitz, B. Soucek, and O. A. Wasson, Nucl. Instr. Methods **53**, 108 (1967).

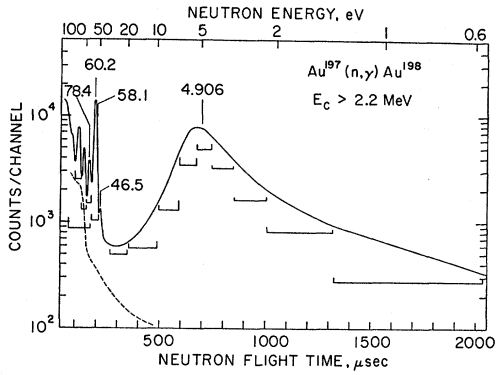

FIG. 1. A flight-time spectrum for $E_c>2.2$ MeV, where E_c represents the energy deposited in the Ge(Li) detector. The dashed curve indicates the background, while the horizontal bars indicate the neutron energy invervals used to obtain γ-ray spectra. The indicated neutron resonance energies are the recommended values of Ref. 20.

III. EXPERIMENTAL RESULTS

A. γ-Ray Spectra

A time-of-flight spectrum for $E_c>2.2$ MeV is shown in Fig. 1, where the quantity E_c represents the energy deposited in the Ge(Li) detector. The low-energy resonances reported by other workers[17–19] are indicated. The brackets below the curve indicate the neutron energy intervals used to obtain γ-ray spectra. The background is indicated by the dashed curve. The vertical axis is the observed counts per 2-μsec flight time interval. The neutron flight time is indicated at the bottom, while the corresponding neutron energy is at the top.

The high-energy part of the γ-ray spectra from thermal capture ($E_n<0.5$ eV) and from capture in various resonances is shown in Fig. 2. The γ-ray peaks labeled with numbers indicate those peaks observed in the thermal spectrum while, except for peak D, the peaks labeled by alphabetic symbols occur in spectra other than thermal. The dashed vertical lines indicate that the γ ray is not observed in that spectrum. The label S in the 4.9-eV resonance indicates a single-escape peak. The labeled γ-ray peaks are due to two-photon escape following pair production while the energy scale refers to the corresponding γ-ray energy. The spectrum from the 60-eV resonance contains a small contribution from the 58-eV resonance, while the 107-eV spectrum contains a small contribution from the 122-eV resonance. For both spectra the contribution of the weaker resonance is 6 or 22% for the thin and thick sample approximations, respectively. The bottom spectrum

[17] R. E. Wood, Phys. Rev. **104**, 1425 (1956).

[18] J. S. Desjardins, J. L. Rosen, W. W. Havens, Jr., and J. Rainwater, Phys. Rev. **120**, 2214 (1960).

[19] J. Julien, S. de Barros, G. Bianchi, C. Corge, V. D. Huynh, G. Le Poittevin, J. Morgenstern, F. Netter, C. Samour, and R. Vastel, Nucl. Phys. **76**, 391 (1966).

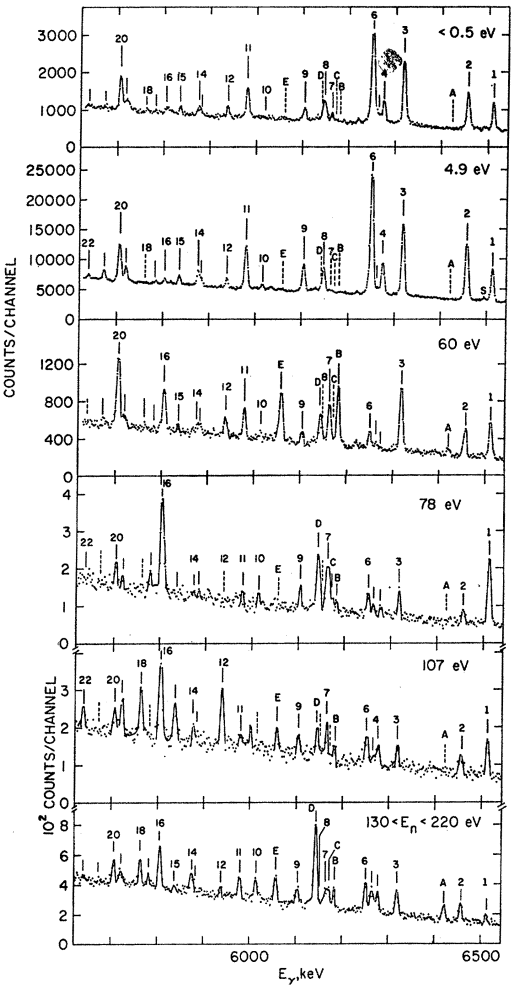

FIG. 2. The high-energy part of the γ-ray spectra for six neutron energy regions. The 4.9- and 78-eV spectra contain contributions from single resonances. The 60- and 107-eV spectra contain small contributions from unresolved resonances, while the bottom spectrum contains contributions from six resonances. The labeled peaks are produced by double-photon escape following pair production, while the energy scale refers to the incident γ ray. The numerical peak labels indicate those γ rays which occur in the thermal ($E_n<0.5$ eV) spectrum, while the alphabetic labels indicate the peaks observed only in the resonances. The solid vertical lines indicate the γ rays which are observed in the corresponding spectrum, while the vertical dashed lines indicate the positions of γ rays which are not observed in that spectrum.

contains contributions from six resonances.[20] Peak 1 is assumed to be the ground-state transition. Spectra obtained from both sides of the 60-eV peak in the time-of-flight spectrum indicate that γ-ray peak A is due to the 58-eV resonance. These spectra also indicate that peak D is more intense than peak B in the 58-eV resonance.

The most striking differences between the spectra are

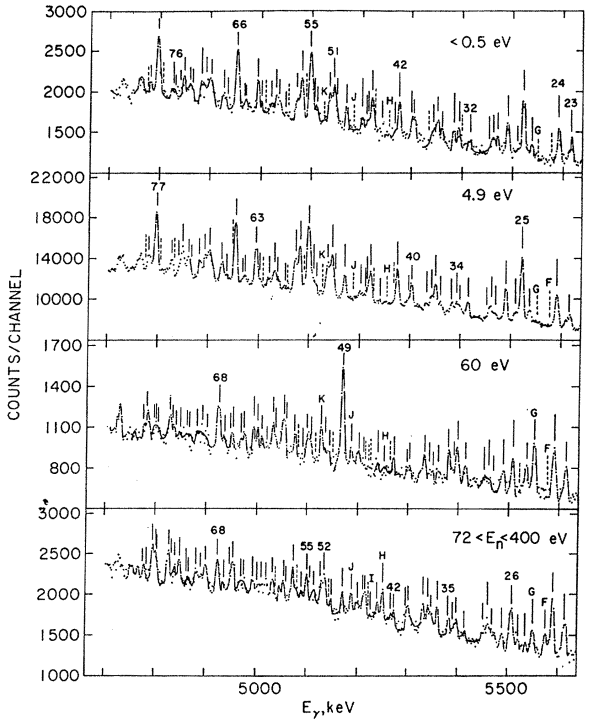

FIG. 3. γ-ray spectra for the four indicated neutron energy intervals for $4.7<E_\gamma<5.1$ MeV. The zero in the vertical scale is suppressed.

the strong variations in individual γ-ray intensities. Peak 6, which is the strongest peak in the 4.9-eV resonance spectrum, is of average intensity in the other spectra. This large fluctuation in partial radiation widths for different capturing states is expected if the partial-width amplitudes are normally distributed with zero mean.[21] Also, the spectra from the resonances contain γ rays which are not observed in the thermal spectrum, e.g., peak E in the 60-eV resonance. The spectra from different resonances aid in identifying weak transitions in a spectrum. For example, peak 5, which is masked by neighboring strong transitions in the 4.9-eV spectrum, is easily identified in the bottom spectrum.

Similar spectra covering the γ-ray energy interval $4.7<E_\gamma<5.1$ MeV are shown in Fig. 3. The zero in the vertical scales is suppressed. The spectra in this region are quite complex. Even with this γ-ray energy resolution, many peaks are unresolved. For $E_\gamma>4.7$ MeV, 78 γ-ray peaks are observed in the thermal spectrum. This is 28 more than was observed in the most recent work of Johnson *et al.*[22] An additional 19 γ rays were observed in the resonance spectra, yielding a total of 97 γ rays. Due to the complexity of the spectra, it is obvious that improved γ-ray energy resolution will reveal many more transitions.

[20] M. D. Goldberg, S. F. Mughabghab, S. N. Purohit, B. A. Magurno, and V. M. May, in *Brookhaven National Laboratory Report No. 325, Suppl. 2* (U. S. Government Printing Office, Washington, D. C., 1966), 2nd ed., Vol. IIc, $Z=61$-87.

[21] C. E. Porter and R. G. Thomas, Phys. Rev. **104**, 483 (1956).

[22] L. V. Johnson, L. B. Hughes, T. J. Kennett, and W. V. Prestwich, Nucl. Phys. **84**, 113 (1966).

TABLE I. Gold γ-ray energies and intensities. Column 1 identifies the γ ray. Numerical symbols label those γ rays which are observed in the 4.9-eV resonance, while alphabetic symbols label those γ rays observed only in other resonances. Column 2 lists the γ-ray energy while Column 3 lists the excitation energy of the final state, assuming all listed γ rays to decay from the capturing state. The remaining columns list the observed γ-ray intensities in units of photons per 1000 neutrons captured for the six different neutron energy intervals listed. Only the statistical contribution to the errors is listed. The known $E1$ transitions are indicated in column 1.

Peak No.	E_γ, keV	E_x, keV	I_j, photons per 1000 neutron captures <0.5 eV	4.9 eV	60 eV	78 eV	107 eV	130–220 eV
1 *E*1	6513.2±0.5	0	12.3±0.5	11.5±0.5	11.1±1.0	17.3±0.8	9.5±0.8	1.9±0.4
2 *E*1	6457.8±0.7	55.4±0.2	17.6±0.8	20.4±0.5	8.4±1.0	2.9±0.4	3.0±1.3	5.4±0.6
A	6421.3±1.1	91.8±0.6	<0.1	<0.1	2.5±0.8	<0.7	<0.7	4.8±0.2
3 *E*1	6320.0±0.7	193.2±0.2	24.8±1.2	23.1±0.5	18.2±1.3	5.0±0.7	4.5±1.2	7.1±0.4
4 *E*1	6276.8±0.8	236.4±0.3	9.1±1.3	10.6±1.1	0.5±0.2	1.7±0.6	5.0±0.6	5.9±0.6
5	6264.9±1.1	248.3±0.6	4.7±0.9	2.5±1.0	1.7±0.3	2.8±0.8	2.3±0.5	7.1±0.6
6 *E*1	6252.6±0.7	260.6±0.2	40.3±1.6	40.0±1.6	4.5±0.5	4.4±1.2	8.5±1.2	7.6±0.5
B	6184.0±0.7	329.2±0.2	<0.2	<0.2	14.6±1.9	2.1±0.8	3.4±1.1	3.7±0.5
C	6173.0±1.5	340.2±1.0	<0.2	<0.2	1.5±0.7	2.4±1.0	<0.7	5.6±0.4
7	6165.5±0.9	347.7±0.4	1.7±0.5	0.4±0.1	11.2±1.7	13.7±1.9	7.6±1.5	4.3±0.4
8	6149.8±0.7	363.4±0.2	6.6±1.6	6.8±0.4	2.6±0.8	<0.6	1.8±0.9	2.0±0.6
D	6145.3±1.1	367.9±0.7	3.0±1.7	<0.6	6.8±0.9	12.6±0.8	7.8±1.3	21.4±1.0
9	6106.7±0.7	406.5±0.2	5.1±0.7	7.9±0.4	3.1±1.0	3.4±0.8	4.6±0.5	4.7±0.5
E	6061.3±0.9	451.9±0.4	<0.2	<0.2	16.2±1.5	1.1±0.6	5.2±0.4	6.6±0.6
10	6017.7±0.9	495.5±0.4	<0.2	0.9±0.3	1.2±0.5	2.2±0.6	<0.7	5.9±0.6
11	5983.3±0.7	529.9±0.2	10.3±0.9	12.6±0.4	6.6±0.9	2.0±0.7	2.9∓0.7	5.9±0.5
12	5941.2±0.9	571.9±0.5	3.2±0.7	2.1±0.3	4.8±0.7	<0.7	12.7±0.6	1.2±0.5
13	5887.2±1.1	626.0±0.6	<0.2	1.8±0.5	2.4±0.6	1.1±0.7	1.1±0.6	<0.4
14	5880.0±0.9	633.2±0.4	3.1±0.8	3.7±0.5	1.5±0.7	1.1±0.7	2.5±0.6	4.6±0.7
15	5839.7±0.8	673.5±0.3	1.6±0.7	2.0±0.3	0.8±0.4	<0.7	7.5±0.8	1.0±0.4
16	5808.2±0.9	705.0±0.4	2.5±0.8	1.3±0.2	10.0±0.4	18.1±1.0	17.3±1.0	9.2±0.4
17	5783.7±1.2	729.5±0.7	0.8±0.4	<0.2	0.6±0.3	3.7±1.0	1.0±0.6	1.9±0.4
18	5766.5±1.3	746.7±0.8	0.9±0.3	0.2±0.1	1.1±0.5	<0.7	9.6±0.6	5.4±0.4
19	5724.3±0.8	788.9±0.3	5.7±1.5	4.5±0.6	3.2±0.8	1.5±0.6	7.0±0.7	2.7±0.4
20	5710.7±0.7	802.5±0.3	11.9±0.8	10.1±0.7	16.0±1.5	4.1±1.0	5.1±0.6	4.4±0.6
21	5677.3±0.9	835.9±0.4	0.5±0.3	2.0±0.4	1.3±0.4	<0.6	<0.6	<0.3
22	5643.4±0.9	869.8±0.4	0.6±0.3	0.9±0.3	<0.3	<0.6	4.0±0.9	0.6±0.3
23	5620.6±0.9	892.6±0.4	3.5±0.8	2.2±0.3	4.6±0.8	5.7±0.5	3.3±0.9	7.1±0.8
24	5594.6±0.8	918.6±0.3	4.3±0.8	5.1±0.3	7.4±1.3	3.5±0.7	5.3±0.9	8.2±0.8
F	5580.6±1.0	932.6±0.5	<0.3	<0.2	<0.3	4.8±0.8	1.4±0.4	3.7±0.6
G	5555.3±0.8	957.9±0.3	<0.3	<0.2	7.5±0.7	2.7±0.8	5.3±1.0	3.0±0.5
25	5539.9±1.0	973.3±0.5	1.8±0.5	1.6±0.5	4.0±0.6	<0.6	1.7±0.8	0.8±0.4
26	5524.4±1.0	988.8±0.5	8.3±0.9	9.0±0.6	0.9±0.3	<0.6	2.6±1.0	1.6±0.5
27	5512.2±1.5	1001.0±1.0	<0.5	1.1±0.5	4.2±0.8	2.1±0.6	5.3±1.2	7.5±0.8
28	5493.7±0.8	1019.5±0.3	4.4±0.9	4.3±0.4	3.2±0.7	3.7±0.8	3.2±1.2	1.3±0.5
29	5474.4±2.5	1038.8±2.0	2.1±0.5	<0.8	<0.3	<0.6	2.6±1.2	3.1±0.5
30	5462.9±0.8	1050.3±0.3	2.3±0.5	2.1±0.3	1.0±0.5	4.9±0.6	3.5±1.2	3.6±0.6
31	5456.0±1.3	1057.2±0.8	0.8±0.4	<0.2	1.1±0.5	7.6±0.6	1.4±0.7	<0.3
32	5418.8±0.9	1094.4±0.4	1.0±0.3	2.2±0.3	2.3±0.8	<0.6	<0.7	1.6±0.5
33	5404.0±1.1	1109.2±0.6	<0.5	1.3±0.3	4.4±1.0	3.3±0.7	2.5±2.5	<0.3
34	5396.6±1.1	1116.5±0.5	2.3±0.5	1.8±0.3	1.2±0.8	<0.6	<0.7	1.2±0.4
35	5387.2±0.9	1126.0±0.4	2.2±0.5	1.8±0.3	3.7±0.9	<0.6	3.5±1.2	3.9±0.8
36	5365.2±1.0	1148.0±0.5	2.2±0.5	1.5±0.3	0.5±0.3	1.8±0.6	1.0±0.7	5.0±0.8
37	5355.0±0.8	1158.2±0.3	3.4±1.5	3.9±0.3	0.5±0.3	1.4±0.6	1.7±1.2	3.5±0.8
38	5346.2±1.0	1167.0±0.5	1.4±1.0	1.8±0.3	0.5±0.4	2.3±0.6	2.5±1.1	1.6±0.6
39	5336.4±1.3	1176.8±0.8	<0.5	0.8±0.3	2.8±1.1	<0.5	2.5±1.4	4.3±1.2
40	5308.0±1.1	1205.2±0.6	2.6±1.0	3.1±0.5	1.4±0.9	1.1±0.4	6.5±1.4	3.4±0.6
41	5303.0±1.5	1210.2±1.0	2.0±0.5	0.6±0.2	1.4±0.9	1.1±0.5	1.4±0.8	1.5±0.6
42	5279.5±0.8	1233.7±0.3	3.8±0.9	4.8±0.4	0.8±0.6	<0.5	<0.7	1.7±0.5
43	5272.1±1.5	1241.1±1.0	0.4±0.2	<0.2	<0.3	1.8±0.6	<0.7	2.9±0.5
H	5256.2±1.5	1257.0±1.0	<0.4	<0.2	<0.3	7.5±0.6	2.5±1.0	4.1±1.2
44	5244.4±1.5	1268.8±1.0	0.5±0.2	<0.2	1.0±0.8	1.3±0.6	3.0±1.2	3.1±0.5
I	5231.3±2.0	1281.9±1.2	<0.5	<0.3	<0.3	<0.7	1.0±0.5	<0.6
45	5226.1±0.8	1287.1±0.3	4.4±0.7	3.8±1.0	<0.3	<0.5	<0.8	0.8±0.5
46	5223.1±1.5	1290.1±1.0	1.4±0.4	0.4±0.2	<0.3	<0.6	<0.8	4.5±0.8
47	5217.8±1.0	1295.4±0.5	1.6±0.6	1.2±0.3	<0.4	1.4±0.6	<0.8	2.8±0.8
48	5206.4±1.0	1306.8±0.5	1.6±0.6	1.2±0.3	1.1±0.4	2.5±0.6	3.3±1.1	1.7±0.6
J	5193.4±2.0	1319.8±1.5	<0.4	<0.2	1.1±0.5	6.6±0.6	<0.8	1.9±0.6
49	5174.7±0.8	1338.4±0.3	2.3±0.8	2.7±0.4	11.3±1.3	3.8±0.9		1.5±0.5
50	5153.5±1.2	1359.7±1.0	0.6±0.3	<0.5	<0.3	1.1±0.5		0.5±0.4
51	5149.9±1.0	1363.3±0.4	4.8±0.6	5.4±0.4	1.1±0.7	<0.6		<0.3
52	5141.1±1.0	1372.1±0.4	3.6±0.6	4.2±0.6	1.1±0.7	14.4±1.4		2.9±0.5
K	5132.1±2.2	1381.1±1.5	<0.3	<0.1	2.6±0.4	<0.6		2.9±0.5
53	5118.7±1.7	1394.5±1.2	1.9±0.3	2.1±0.7	<0.3	<0.8		3.0±0.8
54	5109.5±1.5	1403.7±1.0	1.6±0.3	2.3±0.4	2.7±0.9	<0.8		3.8±0.8
55	5103.0±0.9	1410.2±0.4	9.0±0.6	8.1±0.8	2.5±0.9	<0.8		3.0±0.8
L	5093.8±2.0	1419.4±1.2	<0.4	<0.2	0.7±0.4	<0.8		3.8±0.8
56	5086.3±0.9	1426.9±0.4	5.1±0.4	5.8±0.4	<0.3	<0.6		<0.6

TABLE I. (*continued*).

Peak No.	E_γ, keV	E_x, keV	I_j, photons per 1000 neutron captures <0.5 eV	4.9 eV	60 eV	78 eV	107 eV	130–220 eV
57	5080.9±1.1	1423.3±0.8	2.5±0.4	4.0±0.3	<0.3	4.1±1.0		4.5±0.8
M	5059.5±1.0	1453.7±0.8	<0.1	<0.2	3.6±0.3	0.8±0.6		3.0±0.7
58	5053.7±1.5	1459.5±1.0	0.6±0.2	<0.2	2.3±0.5	2.5±0.8		1.8±0.5
59	5042.5±1.3	1470.7±0.8	1.9±0.7	1.0±0.3	1.0±0.2	<0.5		<0.3
60	5035.2±0.9	1477.9±0.4	1.9±0.7	2.0±0.4	3.7±1.0	<0.5		3.0±0.6
61	5024.6±1.1	1488.6±0.6	1.0±0.6	1.0±0.3	0.4±0.2	5.5±1.0		2.6±0.5
N	5016.6±2.5	1497.0±2.2	<0.4	<0.2	1.3±0.6	<0.7		1.7±0.5
62	5007.5±1.6	1505.7±1.1	0.6±0.4	0.6±0.4	1.3±0.7	<0.7		0.8±0.4
63	4999.1±1.0	1514.1±0.6	3.2±0.8	4.5±0.4	0.9±0.7	5.6±1.0		1.4±0.5
64	4980.5±1.6	1532.7±1.2	0.9±0.3	0.8±0.1	2.1±0.7	5.0±0.8		1.4±0.5
65	4973.1±1.6	1540.1±1.2	0.6±0.3	<0.4	1.4±0.7	1.7±0.8		1.1±0.4
66	4958.2±1.0	1555.0±0.6	6.5±0.8	7.4±0.4	1.3±0.7	10.5±0.6		1.8±0.4
O	4954.2±2.0	1559.0±1.5	<0.4	<0.3	0.8±0.6	<0.8		1.8±0.4
67	4940.3±1.7	1572.9±1.2	0.6±0.4	0.5±0.3	1.4±0.7	<0.4		1.4±0.5
68	4931.6±1.0	1581.6±0.5	1.7±0.7	2.0±0.3	5.9±0.7	1.2±0.7		4.5±0.8
P	4926.6±2.0	1586.6±1.5	<0.3	<0.3	3.1±0.6	<0.6		2.2±0.8
69	4905.5±1.0	1607.7±0.6	3.2±0.7	3.7±0.6	1.3±0.4	3.1±0.7		3.8±0.6
70	4897.4±1.5	1615.8±1.0	2.8±0.7	3.0±0.6	2.6±0.4	<0.6		1.6±0.5
71	4887.5±1.5	1625.7±1.0	2.5±0.8	2.3±0.6	1.7±0.4	7.7±0.8		0.5±0.5
Q	4870.8±1.2	1642.4±0.6	<0.4	<0.3	<0.2	<0.4		1.2±0.5
72	4865.2±1.2	1648.0±0.6	2.4±0.6	2.7±0.4	0.6±0.3	0.7±0.4		<0.4
73	4854.0±1.1	1659.2±0.6	2.8±0.6	3.5±0.6	0.6±0.3	1.7±0.3		4.5±0.6
74	4845.4±2.0	1667.8±2.0	<0.7	1.2±0.6	<0.2	1.7±0.6		<0.4
75	4840.0±1.5	1673.1±1.0	0.4±0.3	<0.3	1.6±0.2	<0.7		0.6±0.4
76	4832.1±1.5	1681.1±0.5	1.1±0.7	1.8±0.4	2.8±0.3	6.0±1.0		2.2±0.6
R	4806.9±2.5	1706.3±2.0	<0.3	<0.3	1.1±0.3	6.0±1.0		4.4±0.6
77	4800.7±1.2	1712.5±0.5	7.7±0.6	7.0±0.3	1.7±0.3	6.0±1.0		4.5±0.8
78	4787.2±1.2	1722.0±0.5	1.6±0.6	1.8±0.3	3.0±0.4	1.0±0.7		<0.4
S	4780.2±1.5	1733.2±1.0	<0.4	<0.3	1.4±0.3	1.0±0.7		<0.4

B. γ-Ray Energies and Intensities

The resulting γ-ray energies and intensities are listed in Table I. Column 1 lists the γ-ray peak number. Column 2 contains the γ-ray energy and its error. Column 3 contains the excitation energy of the final state assuming that each γ ray is a primary transition from the capturing state, and γ ray number 1 populates the ground state. The remaining columns contain the absolute γ-ray intensities in units of photons per 1000 neutrons captured for the various neutron energies. These intensities were not determined independently but were normalized to the thermal intensities measured by Groshev *et al.*[23] The summed intensities of the 10 γ rays for $E_\gamma > 6.0$ MeV observed for thermal capture in this experiment were normalized to the value of 126.2 photons per 1000 captures observed in thermal capture for the same γ-ray energy region by Groshev *et al.*[23]

The γ-ray peak positions and net peak areas were determined from a least-squares fit to the experimental data using a Gaussian peak shape with a linear background under the peak. A detailed account of the energy and intensity determination will be given in a later section.

A comparison of the thermal-capture γ-ray energies and intensities obtained in this experiment with those obtained by Johnson *et al.*[22] and by Groshev *et al.*[23] is given in Table II. The peak numbers are those employed in this experiment. The γ-ray intensities are in photons/1000 captures. The intensities agree quite well, although it must be remembered that the intensities of this experiment were deduced from the intensities of Groshev *et al.*[23] The γ-ray energies from this experiment are generally within the errors of the other experiments. This indicates that there has been no significant systematic error in the energy determination.

C. Energy-Level Diagram

The low-lying energy levels populated by primary transitions from the capturing state are shown in Fig. 4. The levels deduced from this experiment are compared with those deduced by Johnson *et al.*[22] and by Groshev *et al.*[23] The excitation energies from the latter two papers were deduced from the precision measurements of the low-energy thermal γ rays by Hammermesh *et al.*[24] using a bent-crystal spectrometer. The additional levels observed in the present experiment require the reevaluation of the assignments of the low-energy γ rays. Recent measurements of internal-conversion electrons from thermal capture[25,26] used in conjunction with the precision low-energy γ-ray measurements permit the multipolarity of the low-energy transitions to be determined.

[23] L. V. Groshev, A. M. Demidov, and N. Shadiev, Bull. Acad. Sci. USSR, Phys. Ser. **29**, 769 (1965).

[24] B. Hammermesh, J. E. Monahan, and R. K. Smither, Ann. Phys. (N.Y.) **13**, 284 (1961).

[25] V. A. Bondarenko, P. T. Prokof'ev, and L. I. Simonova, Yadern. Fiz. **3**, 193 (1966) [English transl.: Soviet J. Nucl. Phys. **3**, 135 (1966)].

[26] T. V. Egidy, E. Bieber, and Th. W. Elze, Z. Physik **195**, 489 (1966).

TABLE II. Comparison of the γ-ray energies and intensities produced in thermal-neutron capture by three different experiments. The excitation energies E_x result from assuming that all γ rays are due to transitions from the capturing state. The γ-ray intensities are in units of photons per 1000 neutron captures. Only the statistical error is listed.

	This experiment			Johnson *et al.*[a]			Groshev *et al.*[b]		
Peak No.	E_γ, keV	E_x, keV	I_j	E_γ, keV	E_x, keV	I_j	E_γ, keV	E_x, keV	I_j
1	6513.2±0.5	0	12.3	6516(5)	0	8.6	6508(4)	0	12.2
2	6457.8±0.7	55.4±0.2	17.6	6460	56(3)	11.4	6452	56	17.3
A	6421.3±1.1	91.8±0.6	<0.1						
3	6320.0±0.7	193.2±0.2	24.8	6323	193[D]	17.6	6314	194	26.2
4	6276.8±0.8	236.4±0.3	9.1	6278	238	5.9	6272	236	9.2
5	6264.9±1.1	248.3±0.6	4.7						
6	6252.6±0.7	260.6±0.2	40.3	6255	261	28.8	6248	260	41.8
B	6184.0±0.7	238.2±0.2	<0.2						
C	6173.0±1.5	340.2±1.0	<0.2						
7	6165.5±0.9	347.7±0.4	1.7	6168	348	1.5	6158	353	2.8
8	6149.8±0.7	363.4±0.2	6.6	6150	365	7.0	6142	366	9.8
D	6145.3±1.2	367.9±0.7	3.0						
9	6106.7±0.7	406.5±0.2	5.1	6111	405	4.0	6102	406	4.8
E	6061.3±0.9	451.9±0.4	<0.2				6052(7)	456	1.2
10	6107.7±0.9	495.5±0.4	<0.2				6012	496	0.9
11	5983.3±0.7	529.9±0.2	10.3	5984	531	7.7	5983	525	11.5
12	5941.2±0.9	571.9±0.5	3.2	5942	573	3.4	5939	569	5.3
13	5887.2±1.1	626.0±0.6	<0.2	5906	610	0.4			
14	5880.0±0.9	633.2±0.4	3.1	5880	636	2.6	5878	630	4.0
15	5839.7±0.8	673.5±0.3	1.6	5841	675	1.4	5835	673	2.6
16	5808.2±0.9	705.0±0.4	2.5	5812	704[D]	1.9	5805	703	2.8
17	5783.7±1.2	729.5±0.7	0.8	5787	729	0.9	5785(8)	723	0.7
18	5766.5±1.3	746.7±0.8	0.9	5766	749	0.9	5767	741	1.1
19	5724.3±0.8	788.9±0.3	5.7						
20	5710.7±0.7	802.5±0.3	11.9	5713	803	9.1	5709	799	16.9
21	5677.3±0.9	835.9±0.4	0.5	5678	838	1.7	5675(8)	833	1.1
22	5643.4±0.9	869.8±0.4	0.6	5654	862	1.0	5642	866	1.0
23	5620.6±0.9	892.6±0.4	3.5	5619	896	2.2	5615	893	3.9
24	5594.6±0.8	918.6±0.3	4.3	5594	921	3.4	5592	916	5.5
F	5580.6±1.0	932.6±0.5	<0.3						
G	5555.3±0.8	957.9±0.3	<0.3						
25	5539.9±1.0	973.3±0.5	1.8						
26	5524.4±1.0	988.8±0.5	8.3	5524	992	5.8	5521	987	11.7
27	5512.2±1.5	1001.0±1.0	<0.5						
28	5493.7±0.8	1019.5±0.3	4.4	5494	1022	3.3	5492	1016	5.4
29	5474.4±2.5	1038.8±2.0	2.1						
30	5462.9±0.8	1050.3±0.3	2.3	5468	1047	2.6	5467(7)	1041	4.5
31	5456.0±1.3	1057.2±0.8	0.8						
32	5418.8±0.9	1094.4±0.4	1.0	5420	1095	0.9	5416(8)	1092	1.1
33	5404.0±1.1	1109.2±0.6	<0.5	5402	1113	1.1			
34	5396.6±1.1	1116.5±0.5	2.3						
35	5387.2±0.9	1126.0±0.4	2.2	5388	1128	1.1	5390(6)	1118	3.9
36	5365.2±1.0	1148.0±0.5	2.2						
37	5355.0±0.8	1158.2±0.2	3.4	5352	1163	2.5	5350	1158	6.4
38	5346.2±1.0	1167.0±0.5	1.4						
39	5336.4±1.3	1176.8±0.8	<0.5						
40	5308.0±1.1	1205.2±0.6	2.6	5308	1208	3.3	5304	1204	3.6
41	5303.0±1.5	1210.2±1.0	2.0						
42	5279.5±0.8	1233.7±0.3	3.8	5278	1238	2.9	5275	1233	5.3
43	5272.1±1.5	1241.1±1.0	0.4						
H	5256.2±1.5	1257.0±1.0	<0.4						
44	5244.4±1.5	1268.8±1.0	0.5						
I	5231.3±2.0	1281.9±1.2	<0.5						
45	5226.1±0.8	1287.1±0.3	4.4						
46	5223.1±1.5	1290.1±1.0	1.4	5222	1293	3.5	5218	1290	7.1
47	5217.8±1.0	1295.4±0.5	1.6						
48	5206.4±1.0	1306.8±0.5	1.6	5201	1314	1.2	5198	1310	2.2
J	5193.4±2.0	1319.8±1.5	<0.4						
49	5174.7±0.8	1338.4±0.3	2.3	5175	1341	1.7	5170	1338	3.4
50	5153.5±1.2	1359.7±1.0	0.6						
51	5149.9±1.0	1363.3±0.4	4.8	5148	1367	4.2			
52	5141.1±1.0	1372.1±0.4	3.6				5142	1366	9.0
K	5132.1±2.2	1381.1±1.5	<0.3						
53	5118.7±1.7	1394.5±1.2	1.9						
54	5109.5±1.5	1403.7±1.0	1.6						
55	5103.0±0.9	1410.2±0.4	9.0	5101	1414	7.0	5102	1406	13.9
L	5093.8±2.0	1419.4±1.2	<0.4						
56	5086.3±0.9	1426.9±0.4	5.1						
57	5080.9±1.1	1423.3±0.8	2.5	5083	1432	4.9	5081	1427	7.1
M	5059.5±1.0	1453.7±0.8	<0.1						

TABLE II. (*continued*).

Peak No.	This experiment E_γ, keV	This experiment E_x, keV	This experiment I_j	Johnson *et al.*[a] E_γ, keV	Johnson *et al.*[a] E_x, keV	Johnson *et al.*[a] I_j	Groshev *et al.*[b] E_γ, keV	Groshev *et al.*[b] E_x, keV	Groshev *et al.*[b] I_j
58	5053.7±1.5	1459.5±1.0	0.6	5057	1459	0.8			
59	5042.5±1.3	1470.7±0.8	1.9	5045	1470	2.0			
60	5035.2±0.9	1477.9±0.4	1.9	5036	1479	2.5	5032	1476	3.6
61	5024.6±1.1	1488.6±0.6	1.0	5025	1491	2.3			
N	5016.1±2.5	1497.0±2.2	<0.4						
62	5007.5±1.6	1505.7±1.1	0.6						
63	4999.1±1.0	1514.1±0.6	3.2	4998	1518	2.4	4996	1512	5.5
64	4980.5±1.6	1532.7±1.2	0.9						
65	4973.1±1.6	1540.1±1.2	0.6						
66	4958.2±1.0	1555.0±0.6	6.5	4954	1562	4.9	4954	1554	10.7
O	4954.2±2.0	1559.0±1.5	<0.4						
67	4940.3±1.7	1572.9±1.2	0.6						
68	4931.6±1.0	1581.6±0.5	1.7	4930	1585	1.4	4931	1577	1.2
P	4926.6±2.0	1586.6±1.5	<0.3						
69	4905.5±1.0	1607.7±0.6	3.2						
70	4897.4±1.5	1615.8±1.0	2.8	4901	1615	3.9	4904	1604	7.5
71	4887.5±1.5	1625.7±1.0	2.5	4889	1626	3.1	4888(8)	1620	4.3
Q	4870.8±1.2	1642.4±0.6	<0.4						
72	4865.2±1.2	1648.0±0.6	2.4	4866	1650	2.5			
73	4854.0±1.1	1659.2±0.6	2.8	4854	1662	3.1	4853	1655	8.5
74	4845.4±2.0	1667.8±2.0	<0.7						
75	4840.0±1.5	1673.1±1.0	0.4						
76	4832.1±1.5	1681.1±0.5	1.1	4827	1668	0.8	4829(7)	1679	2.0
R	4806.9±2.5	1706.3±2.0	<0.3						
77	4800.7±1.2	1712.5±0.5	7.7				4801	1707	13.1
78	4787.2±1.2	1726.0±0.5	1.6	4795	1721	5.6			
S	4780.2±1.5	1733.2±1.0	<0.4	4781	1735	1.8			

[a] Reference 22. [b] Reference 23.

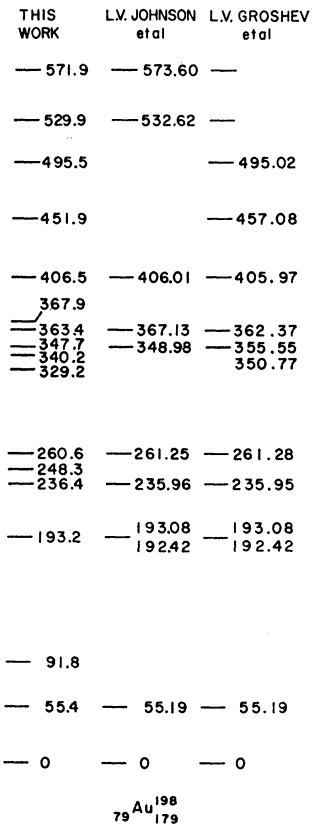

FIG. 4. Gold energy levels populated by primary γ-ray transitions from the capturing state. The excitation energies on the left were observed from resonance-neutron capture in this experiment. The remaining two columns of excitation energies were deduced from thermal-neutron capture in Refs. 22 and 23.

The ground-state spin and parity is 2^-. Egidy *et al.*[26] deduce that the first four excited states observed by Johnson *et al.* and Groshev *et al.* decay to the ground state by $M1$ plus $E2$ admixtures. Thus these states have negative parity and should be populated by $E1$ transitions from the capturing state. No attempt has been made to fit the low-energy γ-ray data or the internal-conversion data into the new levels populated in this experiment. However, the new level at 91.8 keV could decay to the 55.2-keV negative-parity level by a 35.87-keV $M1$ transition.[24] This would suggest that the corresponding 6421.3-keV primary transition has the same multipolarity as the neighboring $E1$ γ rays. The resolution of the present experiment was not sufficient to resolve the two levels proposed by Johnson *et al.* and by Groshev *et al.* at 193-keV excitation which are separated by 0.66 keV.

D. Energy Calibration

The gold γ-ray energies were determined from the thermal-capture γ-ray spectrum produced by a composite sample of gold and natural chromium. The two γ rays from the $Cr^{53}(n,\gamma)Cr^{54}$ reaction at 5999.0±0.6 and 6645.0±0.6 keV as measured by Kane and Mariscotti[27] were used as the energy standards. From these chromium standards and the measured linearity of the

[27] W. R. Kane and M. A. Mariscotti, Nucl. Instr. Methods **56**, 189 (1967); and (private communication).

electronic system, the energy of gold peak numbers 1 and 6 were found to be 6513.2±0.5 and 6252.6±0.7 keV, respectively. The errors contain the statistical error in peak position and system linearity, but not the error in the chromium energy standards.

These two gold γ-ray energies determined from the composite sample were then used as the energy standards in the gold spectra. The remaining gold γ-ray energies were determined relative to the standard lines using the measured linearity of the system and the system gain which was determined from the positions of the calibration peaks and the single- and double-escape peak positions. The resulting gold γ-ray energies are listed in Tables I and II. The listed errors contain only the statistical uncertainty from the γ-ray peak positions and the system gain. The error in the chromium energy standards and systematic errors due to the differential nonlinearity of the analog-to-digital converter have not been included. It is believed that the absolute uncertainty in the γ-ray energies is ±2 keV.

E. Detector-Efficiency Determination

The efficiency of the Ge(Li) γ-ray detector must be known in order to determine the γ-ray intensities from the γ-ray peak areas observed in the ray spectrum. The relative efficiency ϵ_j of the two-photon escape peaks in the detector was determined from a thermal-neutron capture γ-ray spectrum from a natural chromium sample. The experimental geometry, including detector shielding, was identical to that used for the gold sample measurements. Only the γ rays from the $Cr^{53}(n,\gamma)Cr^{54}$ reaction were used in the analysis. The relative γ-ray intensities I_j listed by Kane and Mariscotti[27] were used to determine the relative efficiency from the formula

$$\epsilon_j = A_j/I_j,$$

where A_j is the observed two-photon escape peak area. The resultant relative efficiency as a function of γ-ray energy is shown in Fig. 5. The points represent the experimental values while the solid curve is an eye guide fit to the data. The effect of the γ-ray attenuation in the detector shielding is included in the measurement of the efficiency. The single-escape peak areas were (8±1)% of the double-escape peak areas. For 6.5-MeV γ rays, the full-energy peak area was (1.5±0.5)% of the double-escape peak area.

F. γ-Ray Intensity Determination

The absolute intensity of a γ-ray transition to a final state j is given by

$$I_j = \sigma_{n\gamma j}/\sigma_{n\gamma},$$

where $\sigma_{n\gamma j}$ is the capture cross section for γ-ray emission to state j and $\sigma_{n\gamma}$ is the total-capture cross section. The absolute intensity is obtained from the observed

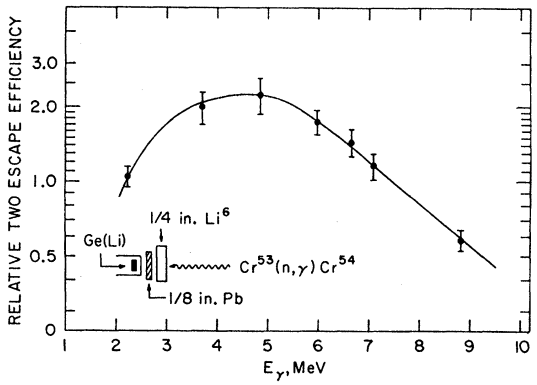

FIG. 5. Relative detector efficiency for two-photon escape peaks following pair production.

γ-ray spectrum by the expression

$$I_j = KA_j/\epsilon_j T,$$

where A_j is the observed γ-ray peak area, ϵ_j is the detector efficiency, T is the total counts in the γ-ray spectrum for $E_c > 2.2$ MeV, and K is a constant independent of both neutron energy and γ-ray energy. This expression assumes that the quantity T is a measure of the number of neutrons captured. Since the constant K is independent of neutron energy, it was evaluated at thermal-neutron energies. The summed intensities of the 10 highest-energy γ rays for $E_\gamma > 6.0$ MeV observed at thermal were normalized to the value of 126.2 photons per 1000 neutrons captured observed by Groshev *et al.*,[23] as mentioned previously. The resulting γ-ray intensities for the various neutron energy intervals are listed in Tables I and II. The listed errors contain the statistical uncertainty in the net peak areas as well as the estimated error in determining the background contribution to the total spectrum.

In addition to the double-escape peaks, the γ-ray spectrum contains single-escape and full-energy peaks which must be identified. The position and intensity of the full-energy peak and single-escape peak were determined for each γ ray. When necessary, the observed double-escape peak area was corrected for the contribution of single-escape or full-energy peaks of lower-energy γ rays. Although the γ-ray spectra shown in Fig. 2 do not extend below 4.7 MeV, no γ-ray peaks for $E_\gamma < 4.7$ MeV were observed with sufficient intensity to contribute significant single-escape or full-energy peaks in the γ-ray region above 4.7 MeV. The γ rays listed in Tables I and II are not due to mistaken identification of a full-energy or single-escape peak.

In order to determine the quantity T, the background contribution to the γ-ray spectrum must be determined. A detailed account of the background determination is given in the Appendix, which shows that the background is less than 30% at the capture cross-section minimum near 30 eV and approximately 20% for neu-

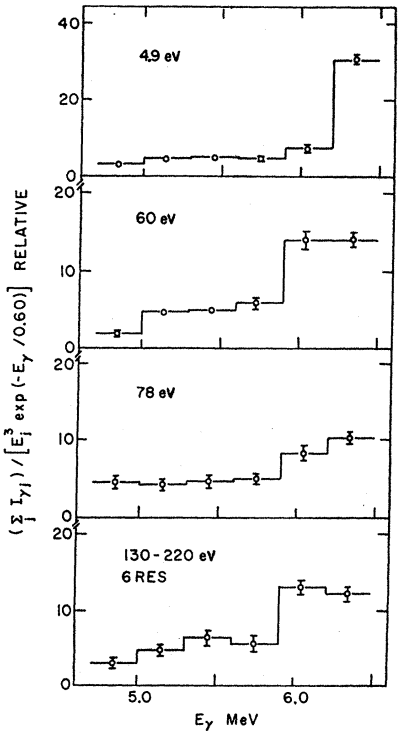

FIG. 6. Reduced γ-ray intensities averaged over 300-keV γ-ray energy intervals.

tron energies greater than 100 eV. The background was small elsewhere.

An anomalous bump has been observed near 5 MeV in the γ-ray spectra from thermal-[11] and kilovolt-[1,2] neutron capture, as well as in the $(d,p\gamma)$ experiments[4] using NaI γ-ray detectors. The bump is not strong in the present spectra. The reduced γ-ray intensities averaged over a 300-keV γ-ray energy interval are shown in Fig. 6. The error bars include only the uncertainty in the summed γ-ray intensities.

The reduced intensity was determined from the expression

$$(\sum_j I_{\gamma j})/[E_j^3 \exp(-E_j/0.60)],$$

where the level density was assumed to have the exponential form with a temperature of 600 keV. The region above 6.0 MeV is strong in all four spectra. If the anomalous bump is present in these spectra, it must occur below 5.0 MeV. This region was not investigated in this experiment. The anomalous bump was also not observed in the thermal-neutron capture γ-ray studies of Johnson *et al.*, who also used a Ge(Li) γ-ray detector. A possible reason for not observing the bump in the Ge detector measurements is the difficulty in determining the γ-ray peak areas in the region near 5 MeV, where the spectrum is quite complex.

IV. INTERFERENCE RESULTS

A. Data Analysis

Let us now turn to the main purpose of this paper, the search for interference effects near the 4.9-eV resonance in gold. This involves the measurement of the variation of individual γ-ray intensities for the neutron-energy interval 0.6–35 eV. First, the process of data analysis will be described.

For low neutron energies in gold where the level width Γ_μ is much less than the energy separating different resonances, the partial-capture cross section for S-wave neutrons $\sigma_{n\gamma j}$ resulting in γ-ray emission to a given final state j may be given by [28]

$$\sigma_{n\gamma j}=\pi(\lambda\lambda^0)\sum_J g(J)\left|D_j^0+\sum_\mu \Gamma_{\mu n}{}^{0\,1/2}\Gamma_{\mu\gamma j}{}^{1/2}/(E_\mu-E-\tfrac{1}{2}i\Gamma_\mu)\right|^2,$$

where λ^0, D_j^0, and $\Gamma_{\lambda n}{}^0$ are evaluated at 1 eV and λ is the incident neutron wavelength, E is the incident neutron energy, J is the total spin of capturing state $=2$ or 1, D_j is the direct amplitude for transition j, μ is the label of various capturing resonances, $\Gamma_{\mu n}{}^{0\,1/2}$ is the reduced neutron width amplitude, $\Gamma_{\mu\gamma j}{}^{1/2}$ is the partial radiation width amplitude for radiative decay of state μ to final state j, E_μ is the resonance energy, Γ_μ is the total width of state, and $g(J)$ is the spin factor $=\frac{5}{8}$ or $\frac{3}{8}$.

The partial cross section which is determined by the coherent sum of a direct amplitude and many resonance amplitudes of the same spin will contain a direct term, a sum of Breit-Wigner single resonance terms, and interference terms. Interference between resonances of the same spin was observed by Coté and Bollinger,[29] while our previous work[30,31] has identified interference between direct and resonance capture. The total-capture cross section $\sigma_{n\gamma}$ is given by the sum of all the partial-capture cross sections

$$\sigma_{n\gamma}=\sum_j \sigma_{n\gamma j}=\pi(\lambda\lambda^0)\sum_J g(J)\times\left[\sum_j D_j^0+\sum_\mu \frac{\Gamma_{\mu n}\Gamma_{\mu\gamma}}{(E_\mu-E)^2+\frac{1}{4}\Gamma_\mu{}^2}\right].$$

For this total-capture cross section, it is assumed that the phases of the reduced neutron width amplitudes and the partial radiation width amplitudes are random so that the interference terms sum to zero. This assumption is reasonable since no interference effects have been reported in total-capture cross-section measurements. For the analysis of the experimental data, it is assumed

[28] A. M. Lane and R. G. Thomas, Rev. Mod. Phys. **30**, 257 (1955).
[29] R. E. Coté and L. M. Bollinger, Phys. Rev. Letters **6**, 695 (1961).
[30] O. A. Wasson, M. R. Bhat, R. E. Chrien, M. A. Lone, and M. Beer, Phys. Rev. Letters **17**, 1220 (1966).
[31] R. E. Chrien, D. L. Price, O. A. Wasson, M. R. Bhat, M. A. Lone, and M. Beer, Phys. Letters **25B**, 195 (1967).

that

$$\sigma_{n\gamma j}/\sigma_{n\gamma} \equiv I_j \propto R,$$

where $R=A_j/T$ and I_j is the absolute γ-ray intensity determined from the γ-ray spectra as described previously. For gold the resonance energies, spins, reduced neutron widths, and total radiation widths of the nearby resonances have been measured. The partial radiation widths of the 4.9-, 60-, 78-, and 107-eV resonances were determined in the present experiment. Thus, except for the amplitude phase factors, the significant resonance amplitudes are determined. After calculating the resonance-resonance interference terms for all combinations of phase factors, any discrepancy between the experimental data and this calculation is attributed to the direct amplitude. In this manner the direct amplitude is extracted from the experimental data by curve fitting.

B. Experimental Data

The variation in γ-ray intensity of 24 selected γ rays is shown in Fig. 7 for neutron energies less than 60 eV. Only those γ rays which were definitely resolved and had sufficient intensity in the 4.9-eV resonance were included in the figure. Each point represents the experi-

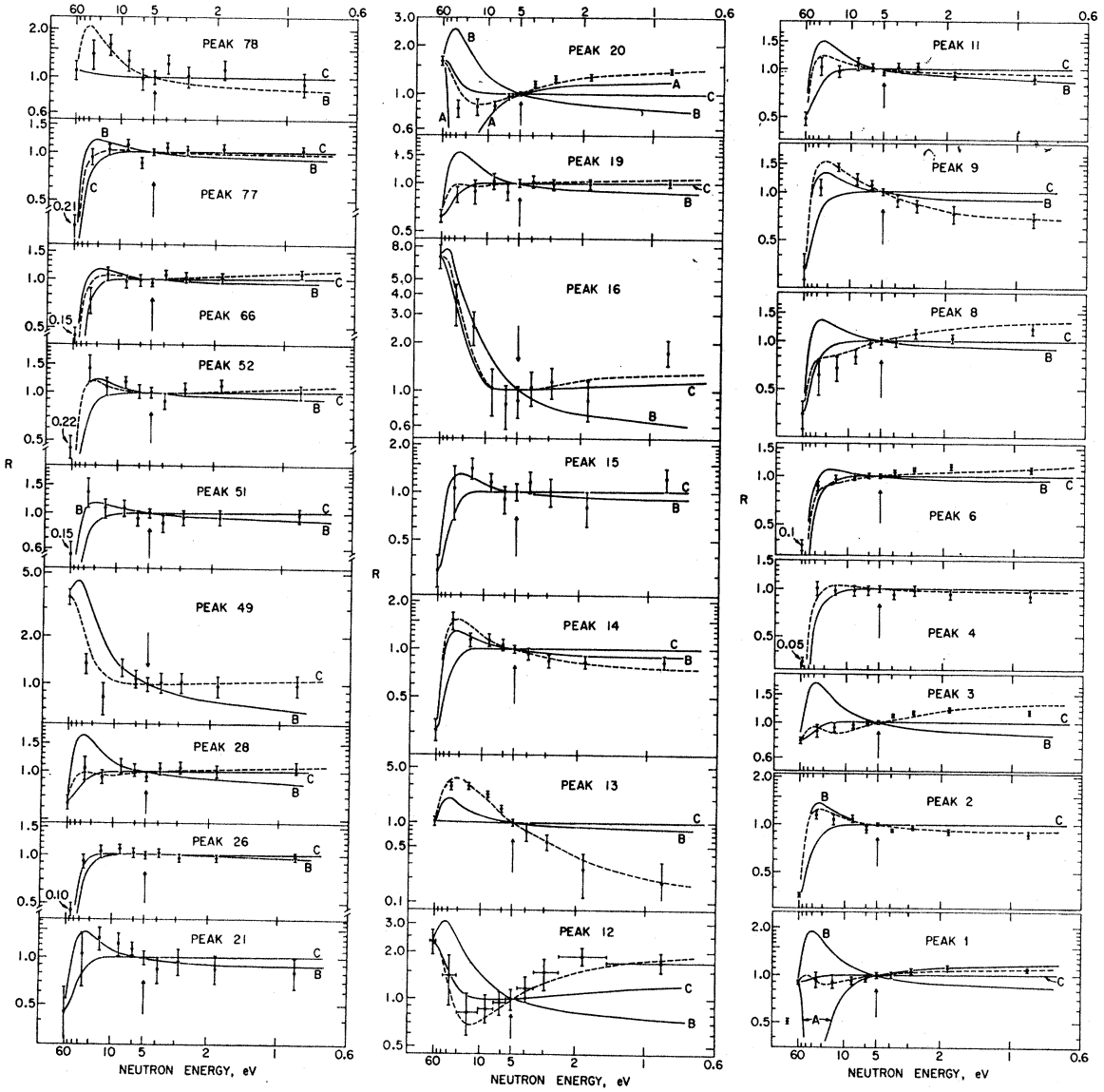

FIG. 7. Relative γ-ray intensity as a function of neutron energy for $E_n<60$ eV. The data points represent the experimental values, while the curves result from various calculations. Curve C results from single-level fits to the 4.9- and 60-eV resonances. Curve B results from resonance-resonance interference between the 4.9- and 60-eV resonances with the amplitude phases chosen to produce constructive interference between the two resonances. The dashed curves which are satisfactory fits to the data result from postulating a bound level.

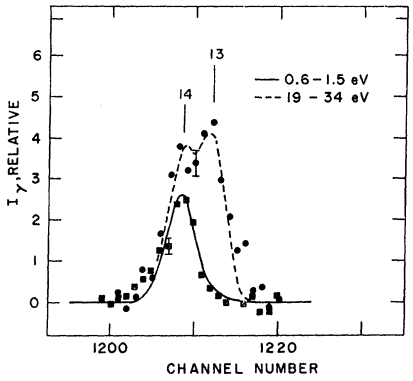

FIG. 8. Comparison of the γ-ray spectra near peaks 13 and 14 for capture of 1- and 25-eV neutrons.

mentally determined relative γ-ray intensity R. The relative intensity for each γ ray has been arbitrarily normalized to unity at 4.9 eV. The 10 neutron-energy intervals used to obtain each datum point are indicated by the horizontal bars for peak 12. The neutron-energy interval $40<E_n<55$ eV was excluded because of the influence of the 46-eV resonance and poor statistics. The relative γ-ray intensities were determined from the net double-escape peak areas as described previously. The indicated errors for each point include the statistical error in determining the net peak area as well as an estimate of the systematic error in determining the background contribution to the total γ-ray spectrum. The vertical arrows indicate the position of the 4.9-eV resonance while the γ-ray peak numbers correspond to the listing of Table I.

In general, the γ-ray intensities varied by about 10% between the 4.9-eV resonance and 0.6 eV. The variation increased for some γ rays and decreased for others in an apparent random manner. Although small in general, these variations are considered significant. However, the intensity variation was quite large for peak 13. For this example, there was a factor of 10 variation in intensity between 1 and 30 eV. This γ ray, which is weak in the 4.9-eV resonance spectrum, is located only 7 keV from the neighboring γ ray. That this variation in intensity is not due to improper peak unfolding is shown in Fig. 8, where the γ-ray spectra near peaks 13 and 14 from neutron capture at 1 and 25 eV are compared. Both spectra were normalized to the same total counts in the spectrum for $E_\gamma>3.2$ MeV. Peak 13 is clearly observed in the 19–34-eV spectrum but is quite weak at 1 eV. The curves in Fig. 8 represent the least-squares fit to the data points.

In order to interpret the observed intensity variations, calculations of the intensity produced by different resonance amplitudes are performed. The various curves in Fig. 7 are proportional to the ratio of the partial-capture cross section to the total-capture cross section. The curves labeled C result from the contribution of only the 4.9- and 60-eV resonances with the interference terms neglected. Due to the large values of the reduced neutron widths of these two resonances, the contribution of other resonances to this neutron-energy region is negligible for the case of no interference. Thus the failure of curve C to fit the experimental data indicated that interference terms are present in the partial-capture cross sections.

C. Sources of Interference

The first source of interference to consider is that between the strong spin-2 resonances at 4.9 and 60 eV. Curve A in Fig. 7 results from the inclusion of the interference between these two resonances with the relative phases of the amplitudes chosen to produce destructive interference between the two resonances. These curves all fall to a value of zero near 30 eV and are shown only for peaks 1 and 20. Curve B results from the opposite choice of phases. None of the data is fitted by curve A, while 7 γ rays are fitted by curve B. Thus, for most γ rays additional sources of interference are required.

The contribution of the other neighboring positive energy resonances are now considered. Except for the partial radiation widths, the parameters of these resonances were taken from the neutron cross-section compilation[19] and are listed in Table III along with the postulated bound level parameters. It is assumed in the analysis that the spin assignments are correct. The partial radiation widths $\Gamma_{\mu\gamma j}$ for the 4.9-, 60-, 78-, and 107-eV resonances were obtained from the corresponding γ-ray intensities I_j of Table I from the relation

$$\Gamma_{\gamma j}=I_j\Gamma_\gamma=0.124I_j,$$

where Γ_γ, the total radiation width, was assumed to have a value of 124 meV for each resonance. The resulting partial radiation widths of the 4.9- and 60-eV resonances are listed in Table IV.

The relative resonance amplitudes for the resonances which are of significance for neutron energies less than 60 eV are shown in Fig. 9. The vertical logarithmic scale represents the magnitude of the quantity $(g\Gamma_n^0)^{1/2}/(E-E_\mu)$, while the horizontal logarithmic scale represents the neutron energy. Each curve, which is labeled with the corresponding resonance energy, represents the relative contribution of each resonance amplitude to the total-capture cross section. The dominance of the 4.9- and 60-eV resonances, as well as the insignificance of the 46-eV resonance for $E_n<40$ eV, is evident. The con-

TABLE III. Resonance parameters used in interference calculation.

J	E, eV	Γ_n^0, meV	Γ_γ, meV
2	−20	4.4	124
2	4.91	7.05	124
1	46.5	0.02	124
1	58.1	0.59	124
2	60.2	9.8	124
1	78.4	1.84	124
2	107	0.75	124

TABLE IV. Partial radiation widths used in gold interference analysis of 24 γ rays. Column 1 lists the γ-ray identification number. Columns 2–4 list the partial radiation widths of the three spin-2 resonances used in the interference analysis of Fig. 7. The signs refer to the relative phases of the partial radiation width amplitudes. Each amplitude of the 49-eV resonance was arbitrarily assigned a positive sign. Columns 5 and 6 list the type of interference observed at 20 and 1 eV, respectively. The +, −, and 0 symbols refer to constructive, destructive, and no interference, respectively.

	Partial radiation widths, meV			Interference	
Peak No.	−20 eV	4.9 eV	60 eV	20 eV	1 eV
1	−1.25	1.43	−1.36	−	+
2	<0.10	2.54	−1.05	+	−
3	−6.3	2.86	−2.28	−	+
4	<0.10	1.32	−0.06	+	−
6	−2.00	4.95	−0.56	+	+
8	−0.90	0.84	−0.32	−	+
9	+0.58	0.98	−0.39	+	−
11	−0.62	1.56	−0.82	+	−
12	−2.6	0.26	−0.60	−	+
13	+2.0	0.22	−0.30	+	−
14	+0.20	0.46	−0.19	+	−
15	<0.10	0.25	−0.10	+	−
16	−1.00	0.16	−1.40	+	+
19	−0.28	0.56	−0.40	0	0
20	−4.5	1.24	−2.00	−	+
21	<0.05	0.25	−0.18	+	−
26	<0.10	1.08	−0.04	+	−
28	−0.20	0.54	−0.40	0	0
49	−0.44	0.33	−1.40	0	0
51	<0.05	0.67	−0.14	+	−
52	−0.21	0.52	−0.14	+	−
66	−0.17	0.92	−0.16	0	0
77	−0.08	0.87	−0.21	0	0
78	<0.03	0.22	−0.37	+	−
Sum	23.81	25.03	14.87		

tributions of the stronger resonances at 58, 78, and 293 eV to the total-capture cross section is <1% at 1 eV and <10% at 40 eV. A direct amplitude, which is not shown in the figure, would be constant and could not be distinguished from the resonances with energies greater than 150 eV, e.g., the 151- and 293-eV resonances.

For the partial resonance amplitudes, the curves in Fig. 9 must be multiplied by the corresponding partial radiation width amplitudes. In order for the spin-1 resonances at 58 and 78 eV to contribute significant interference below 40 eV, their respective partial radiation widths must exceed by a factor of 10 the partial radiation widths of the 4.9- and 60-eV resonances. Except for extreme cases, the spin-1 resonances will contribute only weakly to the partial-capture cross section. Thus the deep minima produced near 30 eV for destructive interference between the 4.9- and 60-eV resonances cannot be removed by the inclusion of the resonances of spin 1. Likewise, the contribution of the spin-2 positive energy resonances to the partial-capture cross section is not sufficient to fit the data. The partial radiation widths of the strong resonances at 151 or 250 eV must also exceed by more than a factor of 10 the partial radiation widths of the 4.9- and 60-eV resonances in order to remove a possible destructive interference so close to the 60-eV resonance as to be unobservable. Such large relative values of the neighboring partial

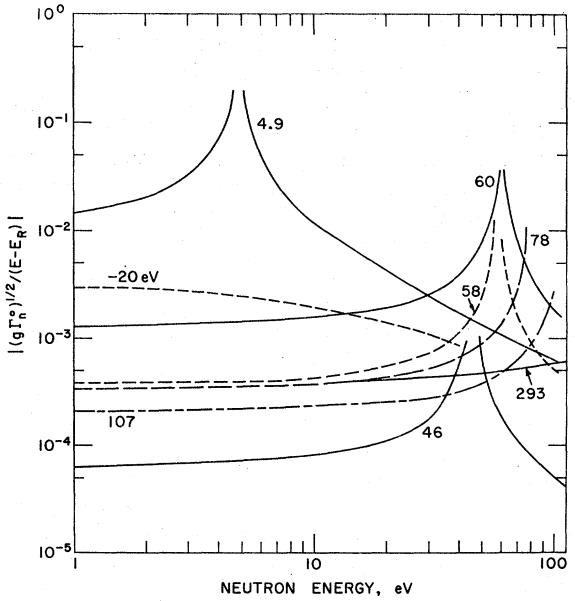

FIG. 9. Relative resonance amplitudes for the resonances which can contribute significantly to the partial-capture cross sections for neutron energies less than 60 eV.

radiation widths are statistically expected only for a few γ rays, namely, those which have small values of the partial radiation width of the 60-eV resonance such as peaks 4 and 26. For all other γ rays such a large relative value is statistically improbable. This leaves only the bound levels or a direct amplitude to produce the required additional interference.

The maximum contribution of the bound levels is determined from the thermal-capture cross section. The measured thermal-capture cross section is 98.8±0.3 b.[20] The calculated contribution from the positive energy resonances is 93.6±3.0 b of which 92.4±3.0 b is due to the 4.9-eV resonance. The error is from the listed uncertainty in the resonance parameters.[20] The difference of 5.2±3.0 b is attributed to the bound levels. Reasonable fits to the data were obtained by postulating a bound level of spin 2 which contributed 3.5 b to the thermal-capture cross section. The position of the bound level was arbitrarily placed at −20 eV, which is consistent with the average level spacing of approximately 23 eV for spin-2 resonances in gold.[18] Assuming the bound level to have the same total radiation width as the unbound resonances then determines the reduced neutron width of the bound level, which is listed in Table III. If more than one bound level is postulated, the restriction on the sum of the fitted partial radiation widths is removed, but the upper limit of 3.5% on the bound-level contribution to the thermal-capture cross section remains. The results obtained by including the postulated bound level as well as the 4.9- and 60-eV resonances in the calculated γ-ray intensities are shown by the dashed curves of Fig. 7, which represent adequate fits to the data. The partial radiation width amplitudes

of the bound level were varied to obtain the best fit to the data. The five peaks without dashed curves are fitted adequately by curve B, which means that the corresponding partial radiation widths of the bound level are small. The results obtained from the interference analysis of the 24 γ rays are listed in Table IV. Column 1 identifies the γ-ray transition while columns 2–4 contain the partial radiation widths in meV for the three spin-2 resonances. The signs were those used for the partial-width amplitudes which were arbitrarily assigned to be positive for the 4.9-eV resonances. Columns 5 and 6 list the experimentally observed interference at 20 and 1 eV, respectively. The + symbol refers to constructive interference; the − symbol indicates destructive interference; and the 0 symbol means no interference.

It is emphasized that the listed parameters of the bound level are not unique, but form one particular set of reasonable parameters which is consistent with the measured thermal-capture cross section and produces the observed variation of γ-ray intensity with neutron energy without the need for a direct-capture cross section.

V. DISCUSSION

The interference anlaysis shows that a reasonable fit to the intensity variation of each of the 24 γ rays can be obtained by considering only the spin-2 resonances at 4.9 and 60 eV in addition to a postulated bound level at -20 eV in the partial-capture cross section. No direct amplitude is required. In order that the sum of the 24 bound partial radiation widths not exceed the corresponding sum for the 4.9-eV resonance, the bound level must contribute $\leq 3.5\%$ of the thermal-capture cross section. As was previously shown, such a contribution is consistent with known level parameters. However, for each γ ray it is required that the phase between the 4.9- and 60-eV resonance amplitudes be such as to produce constructive interference between the two resonances. The phases of the negative energy resonance varied such that its contribution was either constructive or destructive at 30 eV. Such a correlation in phases of the partial radiation width amplitudes between the 4.9- and 60-eV resonances is unexpected, especially since there appears to be no correlation between the respective partial radiation widths. For random fluctuations about half of the interference between the two resonances should be destructive. This failure of any of the 24 selected γ-ray intensities to show a deep minimum near 30 eV is inconsistent with the usual assumptions of compound-nucleus formation.

Two possible experimental causes of the failure to see the minimum at 30 eV are improper background determination for the total γ-ray spectrum and the contribution of thermal-neutron capture in this energy region. An undetected background contribution to the total γ-ray spectrum would tend to decrease the γ-ray intensity and thus enhance the minimum, not destroy it. Thus a possible background error will not explain the failure to observe a deep minimum.

The background measurements have indicated that thermal-neutron capture contributes at most 11% of the observed capture γ-ray spectrum at 19 eV. Using the cross section calculated from the nearby resonances indicated that the thermal-capture contribution at 30 eV would be less than 17%. This 17% thermal contribution could then produce an observed relative γ-ray intensity of 0.20 at 30 eV, even if the partial cross section for 30-eV neutrons were zero. Thus a thermal-neutron background could raise the observed interference minimum to 20% of the no-interference calculation. This contribution is too small to explain the observed data. We conclude that none of the partial-capture cross sections have a value of zero near 30 eV.

The next possible source of error is the calculations. Have significant resonance contributions to the partial-capture cross section been overlooked? To a good approximation, for the case of destructive interference between two widely separated resonances of the same spin, the partial cross section will become equal to zero somewhere between the two resonances. The position of the cross-section minimum depends on the relative magnitudes of the two resonance amplitudes, occurring near 30 eV in gold for those γ rays which have the same intensity in both the 4.9- and 60-eV resonances. The inclusion of other direct or resonance amplitudes of the same spin can only shift the position of the minimum cross section. In order to shift the minimum from the region between the 4.9- and 60-eV resonance, the contributions from the neighboring $J=2$ resonance amplitudes must exceed the contribution from the 4.9- and 60-eV resonances in that region. This requires the partial radiation widths of the stronger resonances to exceed by an order of magnitude the partial radiation widths of the 4.9- or 60-eV resonance. This situation is possible for a few γ rays with weak intensities, such as peaks 4 and 26, but is improbable for all of the other γ rays. Thus for gold only the resonances with spin 1 could fill in the destructive minimum at 30 eV. If the partial radiation widths of the 58- and 78-eV resonances have the same value as the 4.9- and 60-eV resonances, the spin-1 resonances can only produce a 10% contribution to the region of the destructive minimum. In order to remove the destructive interference, the spin-1 partial radiation widths would have to be about 10 times the size of the 4.9- and 60-eV partial radiation widths. Thus for a few γ rays, it is conceivable that the spin-1 partial widths would be large enough to cancel the spin-2 destructive interference, but not for all γ rays. Although the combination of the contribution of thermal-capture γ rays and the spin-1 resonances could fill in about 30% of the spin-2 interference minimum, this combination is not sufficient to explain the experimental data. Thus for most of the 24 γ rays, the phases of the 4.9- and

60-eV resonance amplitudes must be such as to constructively interfere between the two resonances.

The final alternative explanation is that the gold resonance spin assignments[17,19,20] are incorrect. Reversing the spin assignments of the 58- and 60-eV resonances such that the 60-eV resonance had a spin of 1 would prevent the 4.9- and 60-eV resonances from interfering and thus prevent the partial cross section from approaching zero near 30 eV for destructive interference. Using this assumption, interference calculations were repeated for eight γ rays. Only one of the peaks was fitted by including only the 4.9-, 58-, 60-, and 78-eV resonances in the analysis. Bound levels for both spin choices would be required to obtain reasonable fits to the data, although the additional calculations were not performed. Even though the changing of the spin of the 60-eV resonance would eliminate the correlation in phases with the 4.9-eV resonance, it is not believed that the fits to the data would be superior. Since no final states of spin and partiy 0^- and 3^- have been identified for gold, no further information on the spins of the capturing states can be determined from the resonance γ-ray spectra observed in this experiment. There is thus no evidence that the spin of the 60-eV resonance is not 2.

The observed partial-capture cross sections can be explained as interference between the local resonances of spin 2 provided that a bound level is postulated. This is consistent with compound-nucleus formation in the reaction mechanism. However, the required correlation in phases of the partial radiation width amplitudes of the 4.9- and 60-eV resonances without a corresponding correlation in the partial radiation widths is unexplained. The occurrance of the same signs for the reduced width amplitudes for the 4.9- and 60-eV resonances is simply a manifestation of the experimental fact that no deep interference minima are observed between these resonances. The result is surprising in view of the usual assumption of normally distributed reduced width amplitudes. It is remarkable that for the 24 strongest γ rays, no complete destructive interference is observed. Although it is possible that many of the weaker γ rays exhibit destructive interference patterns which we are not able to observe, the behavior of the stronger transitions remains unexplained. There is no *a priori* reason, within the framework of the usual statistical assumptions, to expect the strong transitions to behave differently from the weaker ones. It is not necessary to invoke a direct-interaction mechanism, although it is not possible to distinguish between a bound level at -20 eV and a direct amplitude for most of the γ rays.

Refinements in the conclusions of this experiment will require extending the interference analysis to at least 100-eV neutron energy in order to include an energy interval which includes several resonances. This will require improved neutron energy resolution which was not available with the present experiment. Measurements of the spins and parities of the final states would also leave no doubt as to the resonance spin assignments.

VI. SUMMARY

Previously unreported γ rays were observed in thermal-neutron capture in gold. The γ-ray spectra from capture in various resonances contained additional γ rays that were not present for thermal capture. As a result, additional energy levels were deduced for the Au^{198} nucleus. Previously unobserved interference in the neutron-capture cross sections for γ-ray emission to 24 different final states was observed near the 4.9-eV resonance. The type of interference was independent of γ-ray energy, being constructive for some γ rays at 1 eV and destructive for others. Thus interference effects tend to cancel for groups of γ rays. This fact explains the failure of previous measurements with NaI detectors[11–13] to observe interference near the 4.9-eV resonance. This interference was interpreted as resulting from interference between local resonances by postulating a bound level with reasonable parameters. This result was consistent with compound-nucleus formation, although for 24 of the more intense transitions in the 4.9-eV resonance an unexplained correlation in phases of the partial radiation width amplitudes of the 4.9- and 60-eV resonances was required. No simple direct-reaction mechanism is required in the neutron-capture process for these γ rays, which is in agreement with previous experiments in gold.[4,11–13]

ACKNOWLEDGMENTS

The authors thank Isaac W. Cole, Judy Harte, and Jean Domish for computational assistance, Fred Paffrath and Vito Manzella for maintaining the chopper system, and Hobart Kraner and Marco Jamini for supplying the Ge detector.

APPENDIX: BACKGROUND DETERMINATION

Background is here defined as the contribution to the observed γ-ray spectra which is not due to neutrons of the correct energy captured in gold. The background is grouped into three sources: (a) that which is due to neutrons scattered by the sample, (b) that which is independent of the sample, and (c) that which results from low-energy neutron capture in gold at a flight time corresponding to higher-energy neutrons.

The contribution of these background sources to the observed gold spectra was determined from measurements with the following samples: (a) gold sample with and without a 0.025-in. tungsten absorber in the neutron beam, (b) a 1-in.-thick carbon sample with and without the tungsten absorber, and (c) no sample in the beam.

The natural tungsten absorber contains a strong resonance at 19 eV which selectively removed the 19-eV neutrons from the beam. For this experiment, the no-

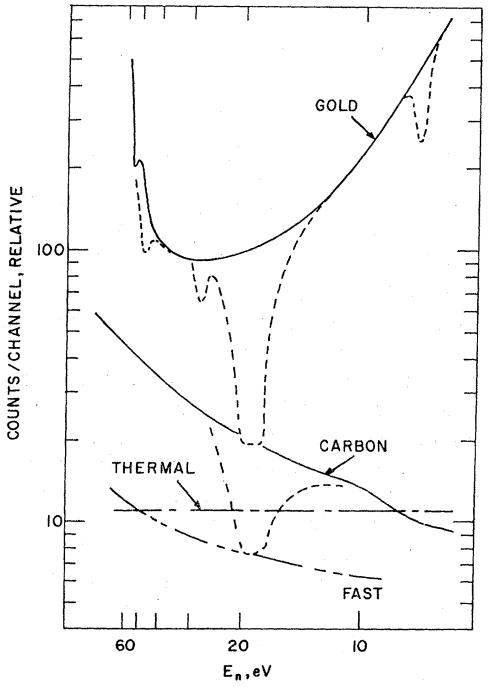

FIG. 10. Gold background determination near the capture cross-section minimum at 30 eV for $E_c > 2.2$ MeV. The solid curve labeled "Gold" is the gold spectrum. The dashed curve is the gold spectrum with the tungsten absorber in the beam. The lower solid curve is the carbon sample spectrum with the dashed curve again resulting from the tungsten absorber. The remaining curves labeled "Thermal" and "Fast" are the backgrounds deduced for the thermal and fast neutrons, respectively.

sample contribution to the background was negligible ($<2\%$) for all energies of interest and will not be discussed further. The background was significant ($\sim 20\%$) for the resonance spectra for $E_n > 100$ eV and for the off-resonance region near 30 eV as is indicated by the dashed curve in Fig. 1. Since the region near 30 eV, where the capture cross section is a minimum, is important for the interference analysis, a detailed discussion of the background determination in this region is given.

The resulting time-of-flight spectra for the neutron-energy region near 30 eV, where the capture cross section has a minimum value, are shown in Fig. 10. The solid curve at the top is the gold spectrum. The dashed curve results from the insertion of the tungsten absorber in the beam. Since the absorber removes all 19-eV neutrons from the beam, the counts observed in the 19-eV dip are not due to 19-eV neutrons, but must be produced either by fast ($E_n \sim 1$ MeV) neutrons which leak through the chopper or by thermal-neutron capture in gold. The lower solid curve represents the carbon spectrum, while the dashed curve again results from the insertion of the tungsten absorber in the beam. The carbon-capture cross section is low so that the contribution of the carbon-capture γ rays are negligible. Thus the 25% contribution in the carbon dip is attributed to the scattering of fast neutrons from the sample. At 19 eV in carbon, 75% of the carbon spectrum is produced by scattering of 19-eV neutrons and the remainder by scattering of fast neutrons. The scattering contribution to the gold spectrum was determined from the carbon spectrum using the known scattering cross sections of both carbon and gold. Due to the uncertainty in the fast-neutron energy spectrum, the calculation of fast-neutron contribution to the gold spectrum is uncertain by a factor of 2. Only 7% of the 18% dip in the gold spectrum can be associated with the fast-neutron background. The 11% difference is attributed to the γ rays from non-19-eV neutron capture in gold. The scattering of 19-eV neutrons contributes an additional 11% to the background, so that at 19 eV the observed gold spectrum contains at most an 18% contribution from neutrons scattered by the sample and an 11% contribution from capture in gold of leak around thermal neutrons. The fast-neutron background and the thermal-capture contribution are indicated by the lower curves in Fig. 10.

The thermal background contribution to the gold spectrum is insignificant outside the internal $15 < E_n < 45$ eV. For $E_n > 40$ eV the background is shown by the dashed line in Fig. 1. The maximum contribution of the background in the total γ-ray spectrum is $\sim 25\%$ in the higher-energy resonances. The background produced by neutrons scattered from the sample contributes only to the continuum region of the γ-ray spectrum, while the leak around thermal capture also contributes to the γ-ray peak areas.